

Kinetic cooling in mid-infrared methane photoacoustic spectroscopy: A quantitative analysis via digital twin verification

ARTICLE INFO

Keywords:

Photoacoustic spectroscopy
Kinetic cooling
Quantum cascade laser
Methane
Digital twin
CoNRad
Relaxation

ABSTRACT

This study presents a detailed quantitative analysis of kinetic cooling in methane photoacoustic spectroscopy, leveraging the capabilities of a digital twin model. Using a quantum cascade laser tuned to 1210.01 cm^{-1} , we investigated the effects of varying nitrogen-oxygen matrix compositions on the photoacoustic signals of 15 ppmV methane. Notably, the photoacoustic signal amplitude decreased with increasing oxygen concentration, even falling below the background signal at oxygen levels higher than approximately 6%V. This phenomenon was attributed to kinetic cooling, where thermal energy is extracted from the surrounding gas molecules rather than added, as validated by complex vector analysis using a previously published digital twin model. The model accurately reproduced complex signal patterns through simulations, providing insights into the underlying molecular mechanisms by quantifying individual collision contributions. These findings underscore the importance of digital twins in understanding the fundamentals of photoacoustic signal generation at the molecular level.

1. Introduction

There is great potential for the development of trace gas sensors based on photoacoustic (PA) spectroscopy for a wide range of applications, such as breath analysis [1], environmental monitoring [2] or safety technology [3]. As an optical method, PAS often utilizes narrowband emitters, e.g. interband cascade lasers (ICLs) [4,5], quantum cascade lasers (QCLs) [6,7] or solid-state lasers [8], ensuring spectral selectivity. Moreover, photoacoustic sensors demonstrate high sensitivity, with the potential to extend even beyond the parts-per-trillion by volume (pptV) range [9]. The use of cost-effective components, such as MEMS microphones and 3D-printed measurement cells [10] or quartz tuning forks [11], and the possibility of realizing miniaturized sensor systems with short optical path lengths [12, 13], highlight the capability of PA technology. However, photoacoustic measurement systems have the drawback that changing measurement conditions, e.g. variations in pressure, temperature, or in particular sample composition, can impact not only the absorption behavior of the sample but also acoustic parameters and the path of non-radiative deactivation, which is crucial for photoacoustic signal generation. This multi-faceted influence of system variables by different physical effects often results in unexpected signal patterns, although only individual measurement parameters are varied [14–16].

Individual calibration of these effects is not a viable approach for transferring the technology from laboratory to real-world applications due to the complexity of their mechanisms. Therefore, we have previously developed an algorithm to predict the cascade of collision-based non-radiative relaxation processes (CoNRad) [17]. This algorithm serves as the core of a digital twin (DT) that additionally considers acoustic and spectral effects and ultimately compensates for all these physical influences on the measurement signal [16]. Given knowledge of all vibrational levels of the molecules in the gas matrix relevant for

signal generation and the lifetimes of all relevant non-radiative relaxation processes, a simple one-point calibration of the sensor under any known measurement condition is sufficient. Additional calibration of the sensor against environmental influences is not required. The functionality of CoNRad and the DT has been validated in collaboration with the German Weather Service (DWD) at a Meteorological Observatory for atmospheric methane monitoring [18]. The results were compared with a cavity ring-down spectrometer G2301 (Picarro, Inc., USA), which is used as a calibrated reference device satisfying the standardization guidelines defined by the European Integrated Carbon Observation System (ICOS) program. Additionally, CoNRad and DT have been compared with a data-driven approach based on partial least squares regression (PLSR), demonstrating performance at least equivalent to that of PLSR [19].

Due to the multitude of possible mechanisms on a molecular level, simple one-dimensional changes in measurement conditions (e.g., the successive addition of another matrix component) often result in unintuitive signal patterns. A special case is the phenomenon of *kinetic cooling*, which can lead to unexpected signal patterns solely due to relaxation effects, even after compensating for all acoustic and spectral effects. Kinetic cooling occurs when, on average, no energy is added to the system during photoacoustic signal generation, but energy is instead removed from the thermal energy reservoir of the surrounding molecules. The term "kinetic cooling" was introduced by Wood et al. in 1971 when investigating the effects of changes in air chemistry on the atmospheric refractive index [20]. While the phenomenon was further studied in the early 1970s using CO₂ lasers and interferometric techniques to examine atmospheric CO₂ levels [21,22], Rooth et al. [23] and Moeckli et al. [24] investigated the impact of kinetic cooling on photoacoustic signal generation during CO₂ detection in the 1990s. Although CO₂ remains the most well-known example of kinetic cooling, the effect has also been observed in the photoacoustic detection of other

<https://doi.org/10.1016/j.pacs.2024.100652>

Received 23 August 2024; Received in revised form 19 September 2024; Accepted 19 September 2024

Available online 27 September 2024

2213-5979/© 2024 The Author(s). Published by Elsevier GmbH. This is an open access article under the CC BY-NC license (<http://creativecommons.org/licenses/by-nc/4.0/>).

gases, such as N_2O [25] and CO [15]. The occurrence of the phenomenon in the photoacoustic detection of CH_4 has also been reported, though in the near-infrared range and without a quantitative analysis of the effect [26,27]. Here, we present for the first time an analysis of this effect, quantifying the contributions of individual collision reactions through digital twin (DT) simulation. This is demonstrated using the example of mid-infrared methane excitation by a quantum cascade laser (QCL) at a wavenumber of 1210.01 cm^{-1} . When adding oxygen to a mixture of 15 ppmV methane diluted in nitrogen, a simple relaxational system with only two molecular states and three relevant transitions is sufficient to quantify the effect of kinetic cooling and to specify the individual contributions of collision reactions.

2. Theory and methods

The foundation of photoacoustic signal generation is built upon molecular collision reactions. During superelastic collisions, internal energy of vibrational states excited after absorption is converted into kinetic energy, known as vibrational-translational (VT) transitions. If the collision partner provides vibrational modes of similar energy, vibrational energy can also be transferred to the collision partner through vibrational-vibrational (VV) transfer processes. The specific pathway of the relaxation cascade of an excited state of the analyte molecule depends on the sample composition, its pressure and temperature, and the periodicity of heat input resulting from the modulation frequency of the emitter. Depending on these parameters, it is possible that the energy absorbed may not be fully converted into kinetic energy within one modulation period, leading to a relaxation efficiency ϵ_{relax} of less than unity. Furthermore, the photoacoustic signal amplitude U_{LIA} , which is the root mean square of the microphone voltage U_{mic} in a PA setup exploiting first longitudinal acoustic resonance and lock-in amplification, respectively, is governed by Eq. (1) [16].

$$U_{\text{LIA}} = \frac{1}{\sqrt{2}} U_{\text{mic}} = C_{\text{cor}} B_{\text{mic}} (\gamma - 1) \underbrace{\frac{Q}{2\pi f_{\text{res}}} \frac{L_{\text{R}}}{V_{\text{R}}} \frac{N_{\text{A}}}{V_{\text{mol}}} N_i \left(\tilde{\nu}_{\text{ph}} \right) P_0 (\tilde{\nu}_{\text{ph}}) \epsilon_{\text{relax}}}_{p_{\text{a}} \left(\tilde{\nu}_{\text{mic}} \right)} \quad (1)$$

This PA signal amplitude, represented as the magnitude of the complex vectorial PA signal, also depends on the optical power of the emitter $P_0(\tilde{\nu}_{\text{ph}})$ and the dimensionless volume fraction N_i of analyte i with an absorption cross-section at the emitted wavenumber $\sigma_i(\tilde{\nu}_{\text{ph}})$.² Besides Avogadro's constant N_{A} and the microphone sensitivity B_{mic} , the measurement signal relies on the molar volume of the sample V_{mol} and the decremented heat capacity ratio $(\gamma - 1)$. It also depends on the length L_{R} , volume V_{R} , quality factor Q , and frequency f_{res} of the acoustic resonator. A refinement factor C_{cor} introduced in [17] must be determined once through a two-point calibration³ when applying a digital twin of the photoacoustic sensor in order to quantitatively converge its virtual space to the physical space [16].

Previous publications have detailed the function of the algorithm for predicting the photoacoustic relaxation cascade [17] and the use of a DT to comprehensively simulate the signal voltage of photoacoustic sensors [16]. In this research, CoNRad and DT were applied to mid-infrared methane excitation using a QCL at 1210 cm^{-1} , and the influence of sample composition on the sensor signal was investigated. For this purpose, the nitrogen:oxygen ($N_2:O_2$) ratio of the bulk matrix was varied while maintaining a constant analyte concentration of 15 ppmV. The QCL was modulated at around 5 kHz with a 50 % duty cycle, resulting in an average optical power of 45 mW. The measurements were conducted

² Assuming that analyte i is the only matrix component absorbing photon energy at $\tilde{\nu}_{\text{ph}}$.

³ Because of a non-zero background signal when applying amplitude modulation, a two-point calibration is necessary. In case of wavelength modulation, a single-point calibration is sufficient.

at slight positive pressure of 1036 mbar and a temperature of $35\text{ }^\circ\text{C}$. The acoustic signal was recorded using an ICS-4270 MEMS microphone (InvenSense Inc., US). The remaining hardware and electronic components of the measurement setup are as described in [7], with the addition of a schematic illustrating the experimental setup. Fig. 1 shows a simple Jablonski diagram of a two-level system comprising the dyad of methane ν_b (black) and the stretching vibration of oxygen ν (red), which are sufficient to understand and quantify the observed effects. The solid arrows illustrate VT processes, while the dashed arrows represent VV processes. A VV transition to nitrogen is considered unlikely due to the large energy gap between the states.

The QCL-excited dyad of methane, encompassing different CH bending modes, can relax to the ground state through collisions with N_2 (k_3) or O_2 (k_4), converting entirely into kinetic energy. Competing with this transfer is an endothermic VV transfer to O_2 (k_1), which removes kinetic energy from the system instead, i.e., the kinetic energy of the collision partners is lower after collision. The inverse energy transfer back to CH_4 (k_2) as well as the VT relaxation of excited O_2 via collision with N_2 (k_5) are shown in grey, as the results indicated they are of negligible relevance. Under the specified measurement conditions, additional transition processes do not need to be considered. Table 1 specifies these collision reactions, including their relaxation rates, and compares them with previously reported values that have been determined by other techniques such as shock tube experiments.

3. Measurements and discussion

Fig. 2 shows amplitude-modulated photoacoustic spectra of 15 ppmV methane diluted in pure nitrogen (yellow) as well as with successive substitutions of nitrogen by oxygen. Refer to the legend of the figure for the assignment of the spectra and their respective O_2 concentrations. The scaled sensor voltage $|U_{\text{LIA}}|$ accounts for changes in P_0 during laser tuning and has been scaled to the maximum optical power at 1209.2 cm^{-1} . This scaling point is extrapolated as a dotted black horizontal reference line across the measured spectrum. Since this scaling occurs outside the methane absorption feature, it corresponds to the photoacoustic background signal (BS), which arises from the interaction of QCL radiation with the windows of the PA cell during amplitude modulation. The purple line represents the absorption cross-section of methane as provided by HITRAN database.

It can be observed that the PA signal decreases with the addition of O_2 , surprisingly this trend continues to a measured magnitude of less than the background signal when exceeding O_2 concentrations of 6 %V. The violet and green spectra at 10 %V and 20 %V O_2 appear to be mirror-

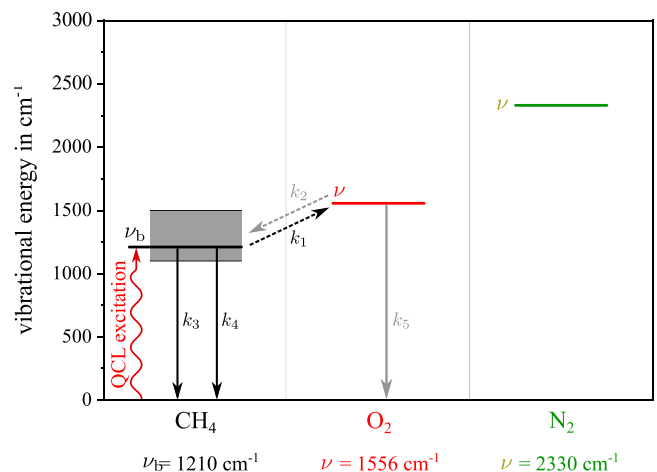


Fig. 1. Simplified Jablonski diagram of a two-level system to predict the relaxation cascade of photoacoustic signal generation for methane monitoring in air. The grey shaded area highlights the dyad of CH_4 vibrations ν_b [28].

Table 1

Processes including rate constants and their energy difference $\frac{\Delta E}{hc_0}$ for the complete de-excitation of methane via collisions with oxygen and nitrogen, respectively. Negative energy differences indicate exothermic collision reactions. Reactions labelled in bold correspond to VT-processes, the others to VV-processes. A (*) indicates the three most important processes identified by DT simulation (refer to Fig. 5).

	Reaction	$\frac{\Delta E}{hc_0}$ in cm^{-1}	Reaction rate k in $\text{s}^{-1}\text{atm}^{-1}$ (used/literature)
(1)*	$\text{CH}_4(\nu_b) + \text{O}_2 \xrightarrow{k_1} \text{CH}_4 + \text{O}_2(\nu)$	+346	$k_1 = 2.53 \times 10^6 / 3.30 \times 10^6$ [29]
(2)	$\text{O}_2(\nu) + \text{CH}_4 \xrightarrow{k_2} \text{O}_2 + \text{CH}_4(\nu_b)$	-346	$k_2 = 3.27 \times 10^7 / 3.27 \times 10^7$ [29]
(3)*	$\text{CH}_4(\nu_b) + \text{N}_2 \xrightarrow{k_3} \text{CH}_4 + \text{N}_2$	-1210	$k_3 = 4.50 \times 10^4 / 8.00 \times 10^4$ [30]
(4)*	$\text{CH}_4(\nu_b) + \text{O}_2 \xrightarrow{k_4} \text{CH}_4 + \text{O}_2$	-1210	$k_4 = 7.00 \times 10^4 / 7.00 \times 10^4$ [29]
(5)	$\text{O}_2(\nu) + \text{N}_2 \xrightarrow{k_5} \text{O}_2 + \text{N}_2$	-1556	$k_5 = 18 / 18$ [31]

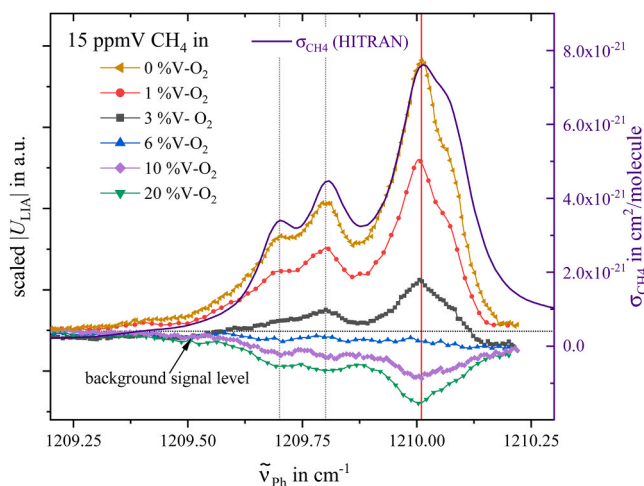


Fig. 2. Amplitude modulated photoacoustic spectra of 15 ppmV methane in pure N_2 (yellow) and successively substituting N_2 by O_2 (red to green). The purple line depicts the absorption cross-section from HITRAN database.

symmetrical to spectra at lower O_2 concentrations. The mirror axis is the dashed horizontal reference line.

To further investigate this phenomenon, an extended series of measurements with 13 different $\text{N}_2:\text{O}_2$ ratios was carried out at a fixed wavenumber of 1210.01 cm^{-1} , indicated by the red vertical line in Fig. 2. Fig. 3 shows the photoacoustic signal of this measurement series in a complex vector diagram with the vector length corresponding to the signal magnitude. The green point cloud illustrates the background signals without methane as the analyte, recorded for each matrix composition, which are constant over all measurements both in amplitude and in phase. The measurement points at the minimum (pure N_2) and maximum (20%V) O_2 concentrations are highlighted in bold.

The projection of the background signal vector onto the signal vector in pure N_2 in Fig. 3 represents its contribution to the measured signal amplitude $|U_{\text{LIA}}(0\%V-\text{O}_2)|$. The red arrow labeled "VV" indicates relaxational losses by vibrational-vibrational energy transfer to oxygen when increasing the O_2 concentration. By successively adding O_2 , the percentage of the background signal in the total signal amplitude increases until signal and background vectors are equivalent. Further increasing the bulk O_2 yields kinetic cooling, visualized by the blue arrow in Fig. 3. As after this threshold, thermal energy is in total removed from the system rather than added. The required energy is extracted from the surrounding molecules in the form of kinetic energy. Consequently, the length of the signal vector becomes shorter than that of the background signal.

To verify that kinetic cooling is responsible for the signal amplitude dropping below the background when increasing the oxygen concentration, the complex PA signals for each measurement were simulated using a digital twin according to [16], and the results (red dots) are compared with the empirical data in Fig. 4. For this purpose, the

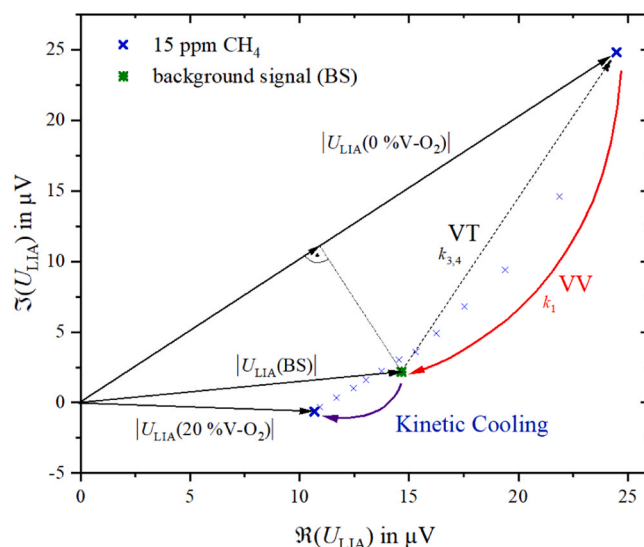


Fig. 3. The photoacoustic measurement signals for 15 ppmV CH_4 at 13 different $\text{N}_2:\text{O}_2$ ratios is presented as a complex vector diagram (blue crosses). The measurement points at the minimum (pure N_2) and maximum (20%V O_2) concentrations are highlighted in bold, while the background signals are shown as a green point cloud. The colored curved arrows illustrate relaxation processes and do not represent vectors.

measured PA signals (blue crosses in Fig. 3) have been offset-corrected with the respective background signals taking the signal phase into account. Fig. 4a illustrates these corrected sensor signals (blue crosses) in a vector diagram and Fig. 4b their absolute values as a function of O_2 concentration.

Plotting these measured and simulated complex signal vectors clearly reveals a 180° phase shift at approximately 6%V O_2 , strongly indicating a transition from effective sample heating to cooling. The further addition of O_2 produces signal vectors in the third quadrant, highlighted in blue in Fig. 4a, indicating the region where kinetic cooling occurs. The DT-simulated signal vectors agree well with the empirical measurements, although the latter are slightly offset and do not pass exactly through the origin of the coordinate system as expected. This discrepancy is likely because each background signal was not recorded immediately after the corresponding measurement signal. Instead, the measurements containing analyte have been carried out in a separate series following a series for all background signals. Fig. 4b shows the amplitude response of the PA sensor with the addition of oxygen, with its intricate pattern attributable solely to relaxational effects. Simulation of signal magnitudes using the DT notably demonstrates that even such complex and unintuitive signal patterns can be reproduced with only minor deviations. This not only aids in understanding the underlying effects and mechanisms on a molecular basis but also eliminates the need for calibrating photoacoustic sensors for such cross-sensitivities.

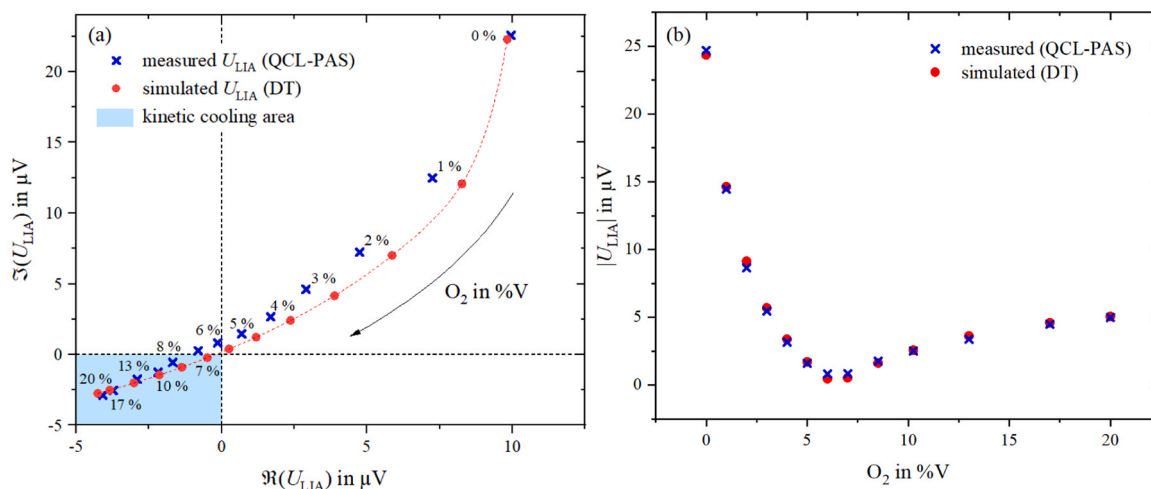


Fig. 4. Measured PA signals from Fig. 3 after offset-correction (blue crosses) and DT-simulated signals (red dots) are presented in a complex vector diagram (a) and their absolute values plotted as a function of O_2 concentration (b).

A valuable additional feature of our algorithmic approach for simulating photoacoustic signals is its ability to quantify the contributions of individual collision reactions to the total PA signal magnitude. Based on this functionality, Fig. 5 displays the contributions to signal generation for selected $N_2:O_2$ matrix compositions as a bar chart. The red dashed horizontal line represents the energy of a photon, i.e. approx. 0.15 eV. The overlaid white diagonally hatched area illustrates the absolute heat dissipation per absorbed photon relative to the maximum possible energy input into the system, q_{100} . The net contribution to photoacoustic signal generation, whether resulting from heat input into the system (indicated by red bars) or heat extraction from the system (indicated by blue bars), is represented in Fig. 5 by the value between 0 eV baseline and the boundary line in q_{100} that the respective filled bars either touch or intersect. The values of net contribution, which indicate whether kinetic heating or kinetic cooling occurs depending on their sign, are displayed on the bars.

The first notable observation in Fig. 5 is that the excited ν_b state of methane can relax and contribute to photoacoustic signal generation only up to approximately 80% (+0.121 eV), even in the absence of oxygen. This results from the fact that the VT relaxation rate k_3 is not sufficiently fast to allow all excited CH_4 molecules to fully relax at a modulation frequency of 5124 Hz. The addition of 1%V O_2 further reduces this net contribution to +0.073 eV, as vibrational-translational (VT) energy transfer via N_2 (red filled bars) competes with vibrational-vibrational (VV) energy transfer to O_2 (blue filled bars), which in return extracts heat from the system. Examining all oxygen-containing compositions reveals that VT via O_2 (red vertically hatched bars) becomes more significant with increasing oxygen content, yet it plays a relatively minor role overall. Analyzing the individual contributions at oxygen concentrations of 6%V and 7%V shows a slightly positive (+0.002 eV) and slightly negative (-0.003 eV) net contribution, respectively, indicating that effective cooling of the system seems to start at an oxygen concentration slightly exceeding 6%V. With a net contribution of -0.026 eV, the sample with the highest oxygen concentration of 20%V clearly demonstrates the effect of kinetic cooling. Theoretical DT-based simulation of a sample in pure oxygen predicts a maximum heat extraction from the system per photon of -0.038 eV. This net contribution is predicted to result from 91% VV cooling and 9% VT heating (via O_2).

4. Conclusion

This work builds on the observation of unexpected signal patterns in amplitude-modulated photoacoustic spectra of methane around

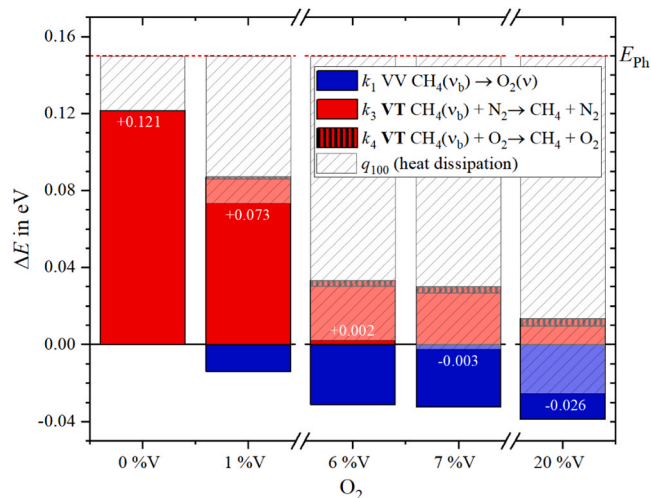


Fig. 5. Representation of the contributions of individual collision reactions to the photoacoustic signal amplitude for selected $N_2:O_2$ matrix compositions as a bar chart. The red dashed horizontal line indicates the energy of a light quantum in eV. The overlaid white diagonally hatched area illustrates the absolute heat dissipation q_{100} .

wavenumbers of 1210 cm^{-1} when varying the $N_2:O_2$ matrix composition. Through extended measurements, the inclusion of phase information from the complex signal, and the application of a digital twin in particular, these signal patterns were successfully interpreted. The phenomenon of kinetic cooling was identified as the cause of the observed drop in signal amplitude below the background level, accompanied by a 180° phase shift. This highlights a significant advantage of analytical models over data-driven models, which require training before they can be applied. As a result, data-driven models would not have been able to interpret unexpected molecular-level measurement effects observed in a single-shot measurement series. Notably, the ability to quantify the contributions of individual collision reactions to photoacoustic signal generation is unique and, to the best of the authors' knowledge, has not been previously reported. The results can be accurately described using a simple two-level system. This study demonstrates that digital twins are not only essential for translating photoacoustic sensor technology from the laboratory to practical applications but also for enhancing the understanding and prediction of fundamental scientific phenomena.

Funding

This work has received essential financial support through the BreathSens project, funded by the German Ministry of Education and Research (BMBF) under grant code 13GW0325C, and the PreSEDA project, funded by the German Federal Ministry for Economics and Climate Action (BMWK) under grant code 03EN2028A. Additional funding was provided by the BayWISS-Health network, supported by the Bavarian Ministry of Research and Arts. The publication fee was covered through funding provided by the DEAL project.

CRedit authorship contribution statement

Frank-Michael Matysik: Writing – review & editing, Validation, Supervision, Methodology, Conceptualization. **Thomas Rück:** Writing – original draft, Validation, Software, Project administration, Methodology, Investigation, Data curation, Conceptualization. **Jonas Pangerl:** Writing – review & editing, Visualization, Software, Project administration, Methodology, Investigation, Data curation, Conceptualization. **Max Müller:** Writing – review & editing, Software, Methodology. **Rudolf Bierl:** Writing – review & editing, Supervision, Project administration, Funding acquisition. **Lukas Escher:** Writing – review & editing, Software, Methodology. **Simon Jobst:** Writing – review & editing, Software, Methodology.

Declaration of Generative AI and AI-assisted technologies in the writing process

During the preparation of this work the authors used ChatGPT in order to improve language and readability. After using ChatGPT, the authors reviewed and edited the content as needed and take full responsibility for the content of the publication.

Declaration of Competing Interest

The authors declare that they have no known competing financial interests or personal relationships that could have appeared to influence the work reported in this paper.

Data availability

Data will be made available on request.

Appendix A. Supporting information

Supplementary data associated with this article can be found in the online version at [doi:10.1016/j.pacs.2024.100652](https://doi.org/10.1016/j.pacs.2024.100652).

References

- [1] S. Weigl, M. Müller, J. Pangerl, T. Rück, Scopes and limits of photoacoustic spectroscopy in modern breath analysis, *Bioanalytical* (2022) 101–159, https://doi.org/10.1007/11663_2022_22.
- [2] A. Zifarelli, R. De Palo, P. Patimisco, M. Giglio, A. Sampaolo, S. Blaser, J. Butet, O. Landry, A. Müller, V. Spagnolo, Multi-gas quartz-enhanced photoacoustic sensor for environmental monitoring exploiting a Vernier effect-based quantum cascade laser, *Photoacoustics* 28 (2022) 100401, <https://doi.org/10.1016/j.pacs.2022.100401>.
- [3] C. Li, K. Chen, M. Guo, X. Zhao, H. Qi, G. Zhang, N. Wang, L. Xu, Intrinsically safe fiber-optic photoacoustic gas sensor for coal spontaneous combustion monitoring, *IEEE Trans. Instrum. Meas.* 71 (2022) 1–9, <https://doi.org/10.1109/TIM.2022.3184343>.
- [4] J. Pangerl, M. Müller, T. Rück, S. Weigl, R. Bierl, Characterizing a sensitive compact mid-infrared photoacoustic sensor for methane, ethane and acetylene detection considering changing ambient parameters and bulk composition (N₂, O₂ and H₂O), *Sens. Actuators B Chem.* 352 (2022) 130962, <https://doi.org/10.1016/j.snb.2021.130962>.
- [5] A. Sampaolo, S. Csutak, P. Patimisco, M. Giglio, G. Menduni, V. Passaro, F.K. Tittel, M. Deffenbaugh, V. Spagnolo, Methane, ethane and propane detection using a compact quartz enhanced photoacoustic sensor and a single interband cascade laser, *Sens. Actuators B Chem.* 282 (2019) 952–960, <https://doi.org/10.1016/j.snb.2018.11.132>.
- [6] K. Kinjalk, F. Paciolla, B. Sun, A. Zifarelli, G. Menduni, M. Giglio, H. Wu, L. Dong, D. Ayache, D. Pinto, A. Vicet, A. Baranov, P. Patimisco, A. Sampaolo, V. Spagnolo, Highly selective and sensitive detection of volatile organic compounds using long wavelength InAs-based quantum cascade lasers through quartz-enhanced photoacoustic spectroscopy, *Appl. Phys. Rev.* 11 (2024), <https://doi.org/10.1063/5.0189501>.
- [7] J. Pangerl, E. Moser, M. Müller, S. Weigl, S. Jobst, T. Rück, R. Bierl, F.M. Matysik, A sub-ppbv-level acetone and ethanol quantum cascade laser based photoacoustic sensor – characterization and multi-component spectra recording in synthetic breath, *Photoacoustics* 30 (2023) 1–12, <https://doi.org/10.1016/j.pacs.2023.100473>.
- [8] S. Qiao, Y. He, H. Sun, P. Patimisco, A. Sampaolo, V. Spagnolo, Y. Ma, Ultra-highly sensitive dual gases detection based on photoacoustic spectroscopy by exploiting a long-wave, high-power, wide-tunable, single-longitudinal-mode solid-state laser, *Light Sci. Appl.* 13 (2024), <https://doi.org/10.1038/s41377-024-01459-5>.
- [9] Z. Wang, Q. Wang, H. Zhang, S. Borri, I. Galli, A. Sampaolo, P. Patimisco, V. L. Spagnolo, P. De Natale, W. Ren, Doubly resonant sub-ppt photoacoustic gas detection with eight decades dynamic range, *Photoacoustics* 27 (2022) 100387, <https://doi.org/10.1016/j.pacs.2022.100387>.
- [10] T. Rück, R. Bierl, F.M. Matysik, Low-cost photoacoustic NO₂ trace gas monitoring at the pptV-level, *Sens. Actuators, A Phys.* 263 (2017) 501–509, <https://doi.org/10.1016/j.sna.2017.06.036>.
- [11] W. Chen, S. Qiao, Y. He, J. Zhu, K. Wang, L. Xiao, Y. Ma, Quasi-distributed quartz enhanced photoacoustic spectroscopy sensing based on hollow waveguide micro-pores, *Opt. Lett.* 49 (2024) 2765, <https://doi.org/10.1364/OL.525188>.
- [12] P. Breitegger, B. Schweighofer, H. Wegleiter, M. Knoll, B. Lang, A. Bergmann, Towards low-cost QEPAS sensors for nitrogen dioxide detection, *Photoacoustics* 18 (2020) 100169, <https://doi.org/10.1016/j.pacs.2020.100169>.
- [13] M. El-Safoury, C. Weber, H. Yassine, J. Wollenstein, K. Schmitt, Towards a miniaturized photoacoustic sensor for transcutaneous CO₂ monitoring, *Sensors* 24 (2024), <https://doi.org/10.3390/s24020457>.
- [14] S. Dello Russo, A. Sampaolo, P. Patimisco, G. Menduni, M. Giglio, C. Hoelzl, V.M. N. Passaro, H. Wu, L. Dong, V. Spagnolo, Quartz-enhanced photoacoustic spectroscopy exploiting low-frequency tuning forks as a tool to measure the vibrational relaxation rate in gas species, *Photoacoustics* 21 (2021) 100227, <https://doi.org/10.1016/j.pacs.2020.100227>.
- [15] J. Hayden, B. Baumgartner, B. Lendl, Anomalous humidity dependence in photoacoustic spectroscopy of CO explained by kinetic cooling, *Appl. Sci.* 10 (2020), <https://doi.org/10.3390/app10030843>.
- [16] T. Rück, M. Müller, S. Jobst, S. Weigl, J. Pangerl, R. Bierl, F.M. Matysik, Digital Twin of a photoacoustic trace gas sensor for monitoring methane in complex gas compositions, *Sens. Actuators B Chem.* 378 (2023) 133119, <https://doi.org/10.1016/j.snb.2022.133119>.
- [17] M. Müller, T. Rück, S. Jobst, J. Pangerl, S. Weigl, R. Bierl, F.M. Matysik, An algorithmic approach to compute the effect of non-radiative relaxation processes in photoacoustic spectroscopy, *Photoacoustics* 26 (2022) 100371, <https://doi.org/10.1016/j.pacs.2022.100371>.
- [18] M. Müller, S. Weigl, J. Müller-Williams, M. Lindauer, T. Rück, S. Jobst, R. Bierl, F.-M. Matysik, Ambient methane monitoring at Hohenpeißenberg utilizing photoacoustic spectroscopy and cavity ring down spectroscopy, *EGU sphere* 2023 (2023) 1–13.
- [19] A. Zifarelli, A.F.P. Cantatore, A. Sampaolo, M. Mueller, T. Rueck, C. Hoelzl, H. Rossmadl, P. Patimisco, V. Spagnolo, Multivariate analysis and digital twin modelling: Alternative approaches to evaluate molecular relaxation in photoacoustic spectroscopy, *Photoacoustics* 33 (2023), <https://doi.org/10.1016/j.pacs.2023.100564>.
- [20] A.D. Wood, M. Camac, E.T. Gerry, Effects of 106- μ laser induced air chemistry on the atmospheric refractive index, *Appl. Opt.* 10 (1971) 1877, <https://doi.org/10.1364/AO.10.001877>.
- [21] L. Sica, Three beam interferometer for the observation of kinetic cooling in air, *Appl. Opt.* 12 (1973) 2848, <https://doi.org/10.1364/ao.12.002848>.
- [22] F.G. Gebhardt, D.C. Smith, Kinetic cooling of a gas by absorption of CO₂ laser radiation, *Appl. Phys. Lett.* 20 (1972) 129–132, <https://doi.org/10.1063/1.1654076>.
- [23] R.A. Rooth, A.J.L. Verhage, L.W. Wouters, Photoacoustic measurement of ammonia in the atmosphere: influence of water vapor and carbon dioxide, *Appl. Opt.* 29 (1990) 3643, <https://doi.org/10.1364/ao.29.003643>.
- [24] M.A. Moeckli, C. Hilbes, M.W. Sigrist, Photoacoustic multicomponent gas analysis using a Levenberg-Marquardt fitting algorithm, *Appl. Phys. B Lasers Opt.* 67 (1998) 449–458, <https://doi.org/10.1007/s003400050529>.
- [25] A.A. Kosterev, Y.A. Bakhirkin, F.K. Tittel, Ultrasensitive gas detection by quartz-enhanced photoacoustic spectroscopy in the fundamental molecular absorption bands region, *Appl. Phys. B Lasers Opt.* 80 (2005) 133–138, <https://doi.org/10.1007/s00340-004-1619-y>.
- [26] F.G.C. Bijnen, F.J.M. Harren, J.H.P. Hackstein, J. Reuss, Intracavity CO laser photoacoustic trace gas detection: cyclic CH₄, H₂O and CO₂ emission by cockroaches and scarab beetles, *Appl. Opt.* 35 (1996) 5357, <https://doi.org/10.1364/ao.35.005357>.
- [27] A. Link, R. Sauter, U. Haas, Highly sensitive and mobile TDL-PA spectroscopic measuring device for methane, *J. Phys. IV* 125 (2005) 841–844, <https://doi.org/10.1051/jp4:2005125194>.
- [28] B. Amyay, M. Louvriot, O. Pirali, R. Georges, J. Vander Auwera, V. Boudon, Global analysis of the high temperature infrared emission spectrum of 12CH₄ in the dyad (ν_2/ν_4) region, *J. Chem. Phys.* 144 (2016), <https://doi.org/10.1063/1.4939521>.

- [29] C. Boursier, J. Ménard, F. Ménard-Bourcin, Vibrational relaxation of methane by oxygen collisions: measurements of the near-resonant energy transfer between CH₄ and O₂ at low temperature, *J. Phys. Chem. A* 111 (2007) 7022–7030, <https://doi.org/10.1021/jp072377y>.
- [30] C. Boursier, J. Ménard, L. Doyennette, F. Menard-Bourcin, Rovibrational relaxation of methane in CH₄–N₂ mixtures: time-resolved IR–IR double-resonance measurements at 193 K and kinetic modeling, *J. Phys. Chem. A* 107 (2003) 5280–5290, <https://doi.org/10.1021/jp034265m>.
- [31] H.E. Bass, Absorption of sound by air: High temperature predictions, *J. Acoust. Soc. Am.* 69 (1981) 124–138, <https://doi.org/10.1121/1.385356>.



Thomas Rück studied Chemistry (Dipl. Chem.) at the University of Regensburg in Germany. In the course of his diploma thesis in cooperation with Continental Automotive GmbH, he started his research on the photoacoustic gas sensing technique in 2009. By now he has 15 years of experience in this field and received his Doctor of Science (Dr. rer. nat.) in 2017. Currently, Thomas Rück is head of the gas sensing team of the SappZ, which is affiliated to the Ostbayerische Technische Hochschule (OTH) of Regensburg.



Jonas Pangerl graduated from the Applied Research program, where he received his master's degree in science (M. Sc.) from the Ostbayerische Technische Hochschule (OTH) of Regensburg in Germany in 2020. Since 2018, he is a member of the Sensorik-ApplikationsZentrum (SappZ) and developed and investigated a photoacoustic trace gas sensor for hydrocarbons. Currently, Mr. Pangerl is pursuing his Doctorate of Natural Sciences (Dr. rer. nat.) in the field of human breath exhale analysis by photoacoustic spectroscopy in cooperation with the Institute for Analytical Chemistry, Chemo- and Biosensorics at the University of Regensburg in Germany.



Lukas Escher received his master's degree in science (M. Sc.) from the Ostbayerische Technische Hochschule (OTH) of Regensburg in Germany, graduating from the Applied Research program in 2023. He currently pursues his Doctorate of Natural Sciences (Dr. rer. Nat.) in the field of photoacoustic spectroscopy in cooperation with the institute for Analytical Chemistry, Chemo- and Biosensorics at the University of Regensburg. Since 2019 he has been conducting research in the field of photoacoustic trace gas analysis, focusing on its application in the UV–vis wavelength range.



Simon Jobst received his master's degree (M.Sc.) at OTH Regensburg in 2015. He is currently pursuing his Doctorate of Natural Sciences (Dr. rer. nat.) in cooperation with the Institute for Analytical Chemistry, Chemo- and Biosensorics at the University of Regensburg and the Sensorik-ApplikationsZentrum (SappZ) in Germany. His research interests include compensation of cross-sensitivities in photoacoustic sensing and developing portable photoacoustic sensors.



Max Müller received his master's degree in electrical and microsystems engineering (M. Eng.) from the Ostbayerische Technische Hochschule (OTH) of Regensburg in Germany in 2020 and his Doctorate of Natural Sciences (Dr. rer. nat.) from the University of Regensburg in 2024, focusing on photoacoustic trace gas sensing, vibrational energy transfer and classical acoustic phenomena. Currently he is working as a research and development engineer for Endress+Hauser.



Rudolf Bierl became Professor at the Ostbayerische Technische Hochschule (OTH) of Regensburg and head of the SappZ in 2009. SappZ is an interdisciplinary thirty-member team mainly dealing with the investigation of various measuring principles and with the development and miniaturization of sensor systems. Mr. Bierl obtained his Diploma degree in Physics (Dipl. Phys.) from the University of Regensburg in Germany in 1991 and his Doctor of Science (Dr. rer. nat.) from the University of Erlangen in 1994. After several deployments in different sectors at Siemens VDO and Continental Automotive GmbH, he was global head of the predevelopment department of sensors at Continental from 2007 until 2009.



Frank-Michael Matysik is Professor of Analytical Chemistry at the University of Regensburg (Bavaria, Germany). He studied chemistry at the University of Leipzig and received his Ph. D. (1994) and "Habilitation" (2001) degrees from the University of Leipzig. From 2001–2008 he was "Privatdozent" for Analytical Chemistry at the same university. In 2008, he accepted the position of a professor of chemistry at the University of Regensburg where he is representing the field of instrumental analytical methods. His research interests include electroanalysis, instrumental analytical developments, chromatographic and electrophoretic separation techniques, mass spectrometry, hyphenated analytical systems, and miniaturized sample preparation techniques.

Thomas Rück^{a,1,*}, Jonas Pangerl^{a,b,1}, Lukas Escher^{a,b}, Simon Jobst^{a,b}, Max Müller^{a,b}, Rudolf Bierl^a, Frank-Michael Matysik^b
^a Sensorik-ApplikationsZentrum (SappZ), Regensburg University of Applied Sciences, Regensburg 93053, Germany
^b Institute of Analytical Chemistry, Chemo, and Biosensing, University of Regensburg, Regensburg 93053, Germany

* Corresponding author.

E-mail addresses: thomas.rueck@oth-regensburg.de (T. Rück), jonas.pangerl@oth-regensburg.de (J. Pangerl), rudolf.bierl@oth-regensburg.de (R. Bierl), frank-michael.matysik@chemie.uni-regensburg.de (F.-M. Matysik).

¹ Equally contributing authors.